Applications Using Fully Automated, Multi-Technique Scanning XPS Equipment Pioneered by Innovative Technology

Maki HASHIMOTO[*1], Miyako TOZU[*1], Masahiro TERASHIMA[*1], Shin-ichi IIDA[*1] and Takuya MIYAYAMA[*1]

[*1]Analytical Solutions Laboratory Product Strategy Dept., ULVAC-PHI, Inc., 2500 Hagisono, Chigasaki, Kanagawa 253-8522, Japan

With the advancements in high-performance materials in recent years, devices combining these materials have become increasingly complex in structure. In particular, the analysis of material interfaces, which play a critical role in device functionality, has gained significant importance. X-ray photoelectron spectroscopy (XPS) has become indispensable as a surface analysis technique. XPS enables precise measurement of the chemical states and elemental concentrations of material surfaces and is widely utilized in the development of battery and semiconductor materials. This article introduces the features and applications of the fully automated, multifunctional XPS system PHI GENESIS.

1. Introduction

In recent years, with the advancement of high-performance materials, the structures of devices combining these materials have become increasingly complex. Consequently, the analysis of material interfaces, which play a critical role in device functionality, has gained significant importance. X-ray photoelectron spectroscopy (XPS) is one of the most commonly used surface analysis techniques for analyzing such interfaces. Because XPS can be used to investigate the chemical states and concentrations of elements present at surface depths of 5 to 10 nm, it is among the most widely used surface analysis techniques.

XPS is capable of analyzing the chemical states and surface compositions of practically all elements, including lithium, which has made it an indispensable tool for developing advanced functional materials, such as those for batteries and semiconductors. Remarkable advances have been made in XPS equipment in recent years, including full automation, enhanced sensitivity, and micro-area analysis. Furthermore, the need to analyze complex material interfaces more quickly and accurately has created a growing demand for equipment capable of applying multiple surface analysis techniques to the same sample. Equipment capable of such functionality is gaining significant attention as a powerful tool to further support materials development.

To meet these needs, we have developed and released the PHI GENESIS system, which features extensive expandability as well as advanced XPS analysis functions. A key feature of this system is its capability to perform in situ measurements with various surface electron spectroscopy techniques, including the following:

(1) Hard x-ray photoelectron spectroscopy (HAXPES)
(2) Ultraviolet photoelectron spectroscopy (UPS)
(3) Low energy inverse photoemission spectroscopy (LEIPS)
(4) Auger electron spectroscopy (AES)
(5) Reflection electron energy loss spectroscopy (REELS)

Furthermore, the following extended functionalities allow for advanced analysis of complex materials.

(6-i) Low-damage depth profiling using cluster ions
(6-ii) Sample heating and cooling
(6-iii) Voltage application inside chamber
(6-iv) Air-free sample transport

Fig.1 shows an image of the PHI GENESIS. Our XPS products are equipped with a scanning X-ray source and high-sensitivity input lens, enabling high-precision quantitative analysis of chemical states in microscopic regions. This has resulted in high praise from many users. This manuscript introduces the latest technologies implemented in the fully automated, multifunctional XPS system PHI GENESIS and details analysis cases where its multifunctionality is utilized.

[*1] Product Strategy Department, ULVAC-PHI, Inc.
(2500 Hagisono, Chigasaki, Kanagawa 253-8522, Japan)

Fig. 1 Exterior of the latest fully automated multi-functional XPS instrument, PHI GENESIS.

2. Features of PHI GENESIS

2.1 Scanning micro-focused XPS

PHI GENESIS uses an ellipsoidal mirror monochromator to monochromatize Al Kα X-rays (1,486.6 eV), enabling it to be focused to a minimum diameter of 5 µm and scanned across an area up to 1.4×1.4 mm on the sample surface. During XPS measurements, scanning X-ray images (SXI) are used to accurately determine measurement positions on a sample. As shown in Fig. 2, the spatial resolution of SXI images in PHI GENESIS is significantly improved over its predecessor—the PHI VersaProbe 4 (minimum diameter: 10 µm).

A Cr Kα X-ray (5,414.8 eV) can be used in addition to the standard Al Kα source as a scanning X-ray source for XPS measurements (Fig.3). These X-rays are generated by irradiating electrons onto a movable Al/Cr dual anode. The generated X-rays are precisely irradiated onto a microscopic point on the sample surface using a dedicated ellipsoidal mirror monochromator for each X-ray source. In addition, independent monochromators with a common focal point are used for the Al Kα and Cr Kα sources, enabling precise alignment of the irradiation point and ensuring optimal performance. Until now, HAXPES measurements using X-ray energies above 5,000 eV had only been possible at large synchrotron facilities such as SPring-8. However, the development of laboratory-based HAXPES systems has made it possible to perform HAXPES analysis with greater information depth in the laboratory[1].

The information depth of HAXPES using the Cr Kα source is approximately three times that of the Al Kα source.

2.2 A new platform for multi-technique XPS

PHI GENESIS is an XPS system that delivers top-level performance while integrating a wide range of analytical techniques into a single instrument. Fig. 4 shows a schematic diagram of the inside of PHI GENESIS when all the described

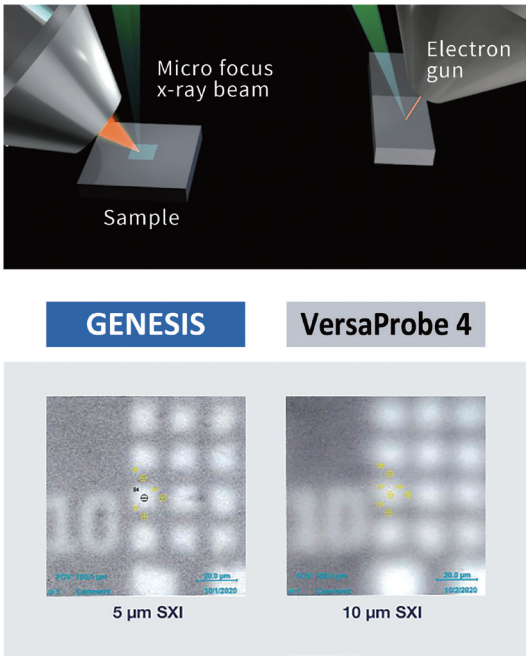

Fig. 2 Schematic diagram of scanning X-ray generation point scanning and irradiation point scanning in PHI GENESIS (above), and the comparison of X-ray excited secondary electron images (SXI: scanning X-ray images) of our conventional model VersaProbe4 (spatial resolution 10 μm) and the new model PHI GENESIS (spatial resolution 5 μm) (below).

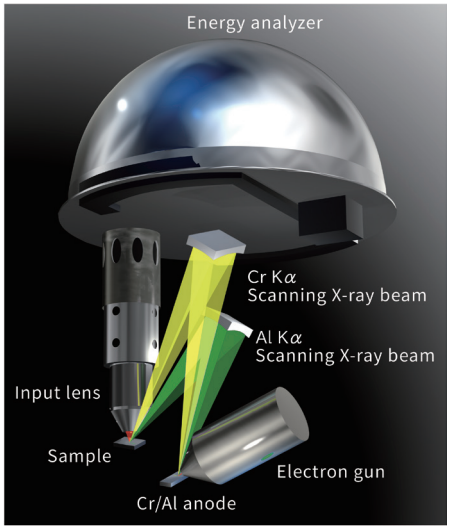

Fig. 3 Schematic diagram of scanning Al Kα XPS and scanning Cr Kα HAXPES in PHI GENESIS.

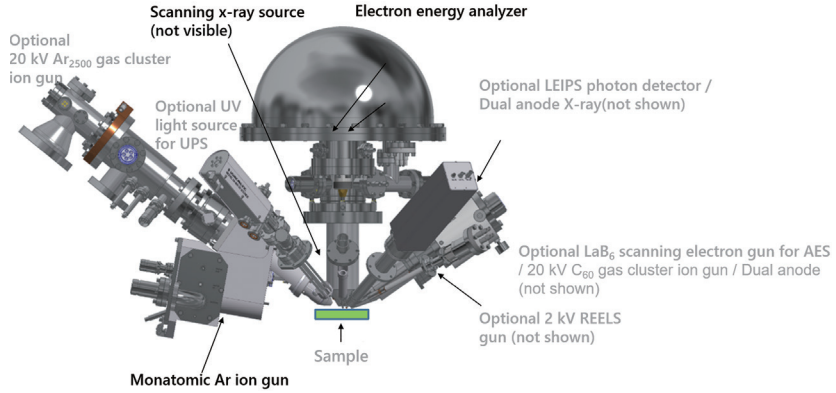

Fig. 4 Schematic diagram of the multi-technique analytical instruments inside PHI GENESIS, showing how each probe and detector captures the analysis point of the sample. Directly above the sample is the electron spectrometer, which is equipped with a hemispherical analyzer and an input lens that collects electrons emitted from the sample. Black text indicates standard specifications, gray indicates options.

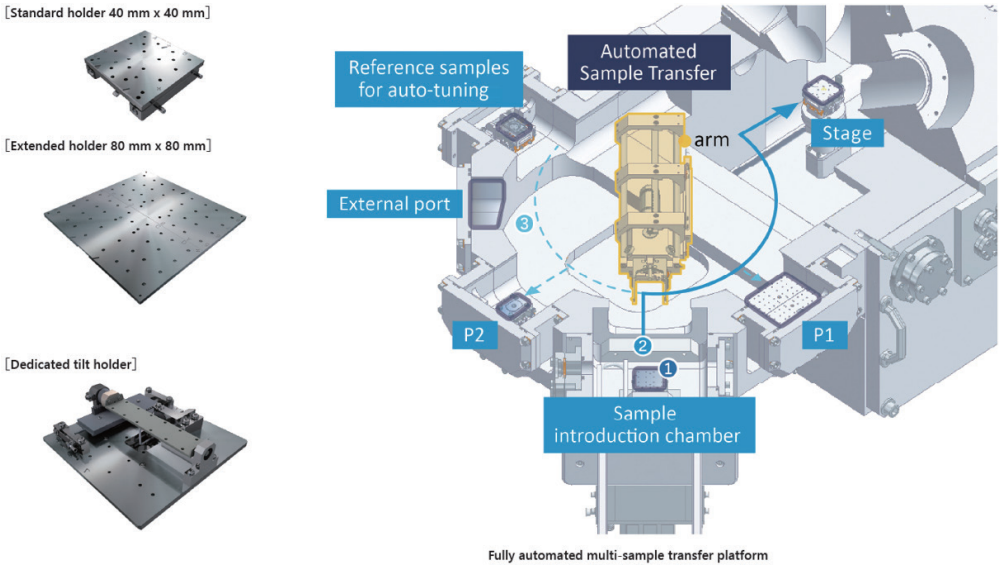

Fig. 5 Schematic diagrams of the PHI GENESIS sample holders (left) and automatic sample transport mechanism (right). When a sample up to 80 mm × 80 mm is placed on the sample holder and inserted into the sample introduction chamber, the sample holder is automatically evacuated and then transported to the analysis position by a robot arm. The sample holder is also fully automatically replaced with the sample holder in the parking lot inside the ultra-high vacuum analysis chamber.

techniques are installed. In the figure, the probes and detectors of each analytical technique are shown facing a single point on the sample for in situ measurements. Directly above the sample is the electron spectrometer, which is equipped with a hemispherical analyzer and an input lens that collects electrons emitted from the sample. Black text indicates standard specifications, while gray indicates options.

It is possible to simultaneously install a UV light source for UPS, a low-energy electron gun and photon detector for LEIPS, and an electron gun for REELS. Each of these provides specific information, such as ionization potential and work function in the case of UPS, electron affinity for LEIPS, and surface electron loss features and bandgaps for REELS. The above techniques provide a complete analysis of energy band structure.

AES offers even higher spatial resolution (approx. 100 nm) than the micro-focus XPS (spatial resolution: 5 µm) provided by PHI GENESIS, enabling surface analysis of even finer regions.

Sample surface cleaning and depth profiling can be performed using an Ar-ion gun. Furthermore, use of an Ar gas cluster ion gun enables low-damage depth profiling and is essential for analyzing organic materials.

In this way, PHI GENESIS enables multi-technique analysis within a single system, which will be particularly effective in the field of new materials development.

Fig. 5 shows a schematic diagram of the various sample holders and the sample transport system. When a sample is placed on the sample holder and inserted into the sample introduction chamber, the sample holder is automatically evacuated and then transported to the analysis position by a robot arm. The sample holder is also fully automatically replaced with the sample holder in the parking lot inside the ultra-high vacuum analysis chamber.

Angle-resolved measurements—which are an effective method for conducting non-destructive analysis of element concentration distribution in the depth direction of a sample—can be performed automatically by adjusting the tilt angle between 0 and 90 degrees from the sample normal direction by means of a motorized sample stage. This method makes it possible to obtain non-destructive, highly accurate depth direction information.

Furthermore, in addition to accommodating large samples up to 80 mm × 80 mm, various options can be added, including heating and cooling mechanisms and an air-free sample transfer system. This makes it easy for users to customize the system and expand its functions to meet their objectives, making the system adaptable to a wide range of research needs.

3. Examples of applications

This section introduces examples of applications in key fields such as batteries, semiconductors, and OLED.

3.1 Battery materials

All-solid-state batteries (ASSBs) have garnered increasing attention in recent years for their advantages over conventional liquid-electrolyte lithium-ion batteries in terms of energy density, safety, and battery life, and are expected to find applications across a wide range of fields, including electric vehicles and sensors. However, further practical application will require overcoming the high internal resistance at the interface between the solid electrolyte and the electrodes, which limits the smooth transport of Li ions.

A battery is a device in which various materials are combined to function together. High-performing batteries require the ideal combination of cathode, electrolyte, anode, and current collector, as well as precise interface control. This makes it particularly necessary to understand the composition and chemical state of interfaces when developing batteries.

In this experiment, a thin-film all-solid-state battery was used that consisted of a lithium metal anode, lithium phosphorus oxynitride (LiPON) for the solid electrolyte, and lithium cobalt oxide ($LiCoO_2$) for the cathode (Fig. 6). In this sample, internal resistance was confirmed at the interface between the solid electrolyte and cathode. Therefore, a sample from prior to the deposition of the lithium metal anode was used for analysis. Table 1 shows a summary of the samples used in this section.

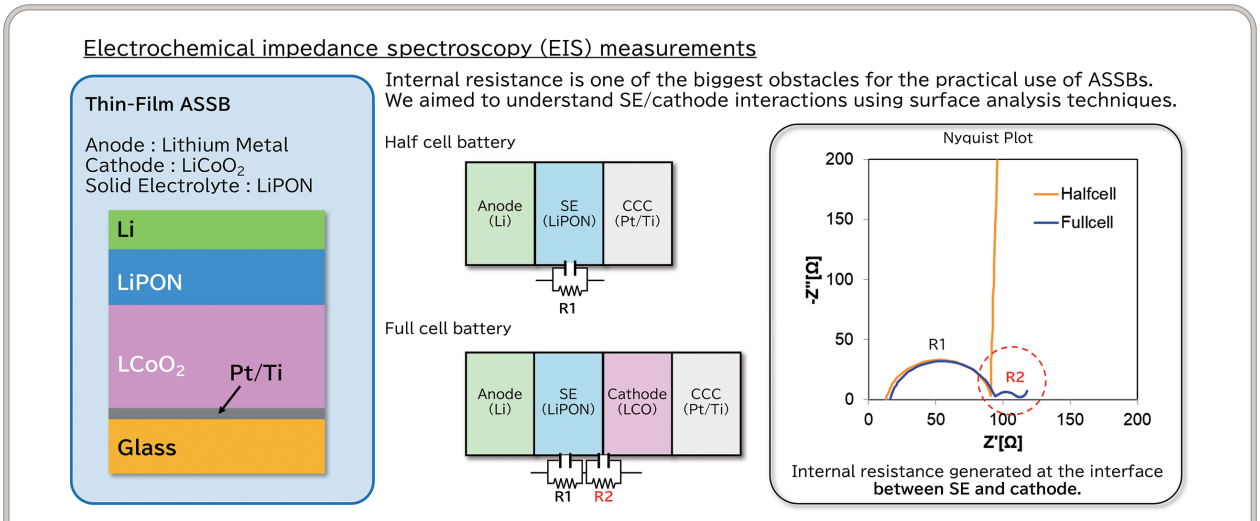

Fig. 6 Schematic diagram of the structure of a thin-film all-solid-state lithium battery model sample, and the issue of interface internal resistance.

Table 1　Description of ASSB samples.

Section	Measurement	Details of Sample
3.1.1	XPS depth profiling	LiPON (2 μm)/ $LiCoO_2$ (5.6 μm)/Pt/Ti/Glass
3.1.2	AES mapping	Cross-section of LiPON (2 μm)/$LiCoO_2$ (5.6 μm)/ Pt/Ti/Glass
3.1.3	in-situ sample heating in XPS chamber	LiPON (100 nm)/ $LiCoO_2$ (5.6 μm)/Pt/Ti/Glass

In this manuscript, we introduce an example where the composition and chemical state of an interface is analyzed using PHI GENESIS. This manuscript also presents results on how deposition temperature affects the interface, evaluated by using the system's heating option to simulate the temperature increase during film formation.

3.1.1　Cross-sectional observation using AES

We first observed two cross-sections of LiPON/$LiCoO_2$ by using AES. To prevent exposure to atmosphere, focused ion beam (FIB) processing was performed in a vacuum[2], after which the sample was transferred to PHI GENESIS using the air-free sample transport system. Fig. 7 shows, from left to right, a schematic diagram of FIB processing, a lithium chemical state map overlaid on an SEM image, and the results of the Li KVV spectra. The chemical state map reflects intensity distributions at 42 eV (LiPON) and 31 eV ($LiCoO_2$) on the spectrum. The obtained chemical state map clearly reflects the difference in the chemical state of lithium between LiPON and $LiCoO_2$, marking the first successful visualization of this difference[3].

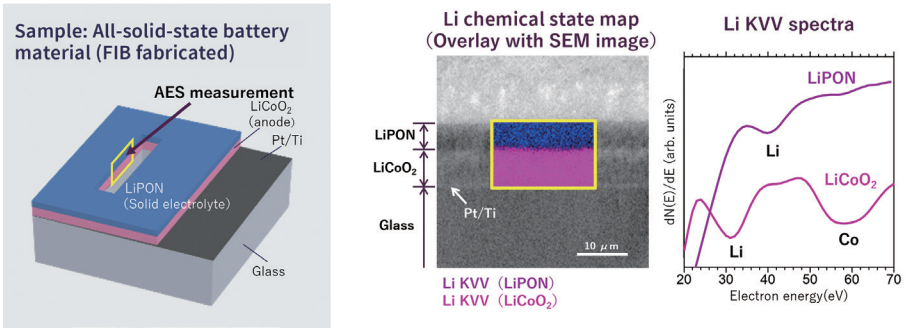

Fig. 7　Schematic diagram of cross-section of all-solid-state lithium battery, Li chemical state map by AES, and Li KVV spectra.

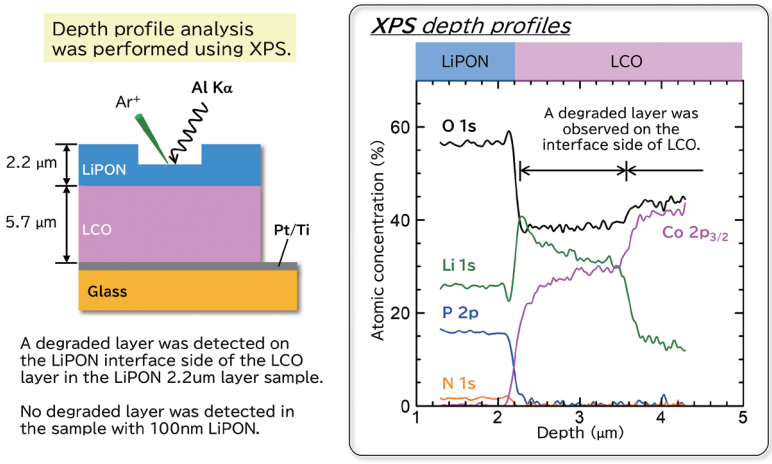

Fig. 8　Schematic diagram of depth profile (depth direction analysis) of thin-film all-solid-state lithium battery model sample, and depth profile showing composition changes of O, Li, Co, P, and N elements near the interface.

3.1.2 Depth profiling using XPS[4)]

Fig. 8 shows the results of depth profiling of a thin-film all-solid-state lithium battery sample by using XPS. Here, only the vicinity of the LiPON/$LiCoO_2$ interface, which is of interest, is displayed. The horizontal axis was calculated based on the time required for sputtering a 2.2 µm-thick LiPON layer and a 5.7 µm-thick $LiCoO_2$ layer. From the XPS depth profile, oxygen enrichment (depth: 2.0 µm) was observed on the LiPON side of the depth interface, while oxygen deficiency (depth: 2.2 to 3.4 µm) was observed on the $LiCoO_2$ side. This phenomenon was not observed after thinning the LiPON layer.

3.1.3 In-situ measurement using internal heating[4)]

Next, LiPON thickness was set to 100 nm in order to evaluate the initial stage of film formation, during which the reaction that occurred between LiPON and $LiCoO_2$ was investigated in detail. Fig. 9 shows the XPS spectra of Co $2p_{3/2}$ and O 1s on a 100 nm-thick LiPON/$LiCoO_2$ surface before heating. There have been numerous reports on the chemical state of LiPON. The O 1s spectra from LiPON are attributed to three components: P=O (non-bridging oxygen), Li^+–O–P (bridging oxygen), and P–O–P (bridging oxygen). Despite the LiPON layer being only 100 nm thick, several percent of cobalt was still detected. This is due to surface irregularities of approximately 100 nm on the $LiCoO_2$ layer. In addition, a satellite peak derived from Co^{3+} was barely detected in the Co $2p_{3/2}$ spectrum. This indicates that the trivalent state is still maintained even after deposition of the 100 nm LiPON layer.

Next, the 100 nm-thick LiPON/$LiCoO_2$ was heated at 200°C for 2 hours inside the XPS chamber. These heating conditions simulate the rise in substrate temperature that occurs during the deposition of 2.2 µm-thick LiPON. After heating the sample, it was returned to room temperature and XPS measurement was carried out once more. The results indicated that the satellite peak of trivalent Co disappeared and metallic cobalt appeared. When the same heating (200°C for 2 hours) was applied to $LiCoO_2$, the Co^{3+} satellite did not disappear, nor did Co^{0+} (metallic Co) appear. This indicates the occurrence of some kind of reaction between LiPON and $LiCoO_2$.

Table 2 Atomic concentration of 100 nm-thick LiPON/$LiCoO_2$ surface before and after heating.

	Atomic concentration (%)				
	Li	P	N	O	Co
Before heating	24	15	7.3	52	1.8
After heating	24	14	6.9	53	2.8

In addition, Table 2 shows the quantitative results (at%) for Li, N, P, O and Co based on the XPS spectra from before and after heating. The N/P ratio remained unchanged at 0.49 before and after heating, while the O/P ratio increased from 3.5 before heating to 3.8 after heating. This indicates the absorption of oxygen by LiPON. Also, considering the decrease of P-O-P and the increase of P=O after heating as shown in Fig. 9, it is suggested that some bridging oxygen was converted into non-bridging oxygen, for which additional oxygen may have been required. Furthermore, assuming that the oxygen was captured from $LiCoO_2$, this would be consistent with the reduction of cobalt and would explain the interfacial oxygen behavior observed in Fig. 8.

In this manner, XPS analysis revealed that the temperature rise during deposition altered the structure of LiPON, causing LiPON to absorb oxygen from $LiCoO_2$ and reducing the cobalt from trivalent to zero-valent. The side reaction occurring at the solid electrolyte/cathode interface impedes the reversible transport of

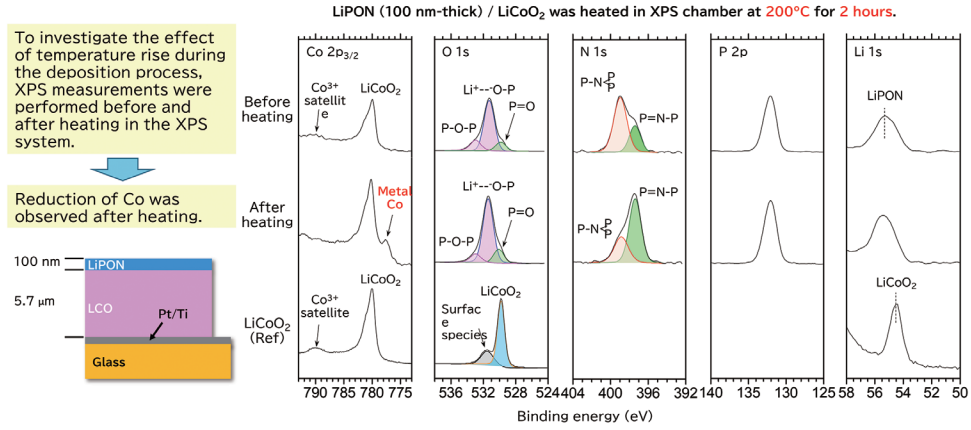

Fig. 9 Schematic diagram of heating of thin-film all-solid-state lithium battery model sample in the device, and XPS chemical state spectra of Co 2p, O 1s, N 1s, P 2p, and Li 1s elements before and after heating. XPS spectra of $LiCoO_2$ are also shown for reference.

lithium ions. This is presumed to be one of the main causes of interface resistance.

3.2 Semiconductor materials (aluminum/silicon oxide laminated films)

The silicon oxide film controls the flow of electrons at the transistor gate, contributing to increased switching speed and reduced power consumption. It also acts to protect the device from the external environment. In particular, SiO_2 has excellent insulating properties and protection performance, and non-destructive analysis using HAXPES and angle-resolved XPS is essential for improving its quality.

3.2.1 Evaluations of semiconductor thin films using a combination of HAXPES and angle-resolved depth profiling

In the case of multilayer structures, detailed analysis of each layer must be performed to confirm that layers are stacked with the intended thicknesses and to check for any diffusion or segregation between layers. Utilizing ion beam sputtering for XPS makes it possible to analyze regions beyond the information depth of XPS alone. However, it is difficult to accurately analyze the sample in its original state because sputtering with a monoatomic ion beam may damage the sample. To solve this problem, we attempted non-destructive analysis in a deeper region by using a Cr Kα source.

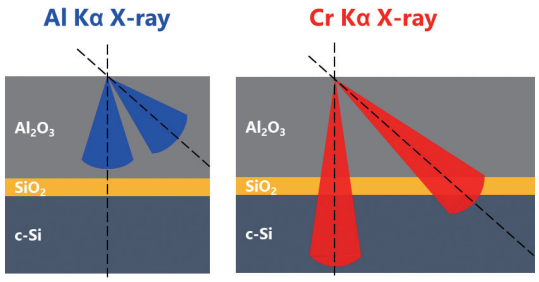

Fig. 10 Difference in information depth between XPS and HAXPES depending on angle.

When investigating the compositional distribution of a thin film or oxide film in the surface depth direction, the information depth of the acquired spectra can be adjusted by changing the angle between the sample surface and the detector (take-off angle). By combining angle-resolved measurements with HAXPES, non-destructive depth profiles can be obtained at greater depths than with XPS alone (Fig. 10).

A combination of angle-resolved depth profiling and HAXPES measurements were performed on a sample with approximately 15 nm of Al_2O_3 deposited on a Si substrate. When this sample is annealed, a passivation (protective) layer of SiO_2 is formed at the interface. The thickness of this passivation layer can be controlled by changing the annealing temperature. The Al_2O_3 surface layer

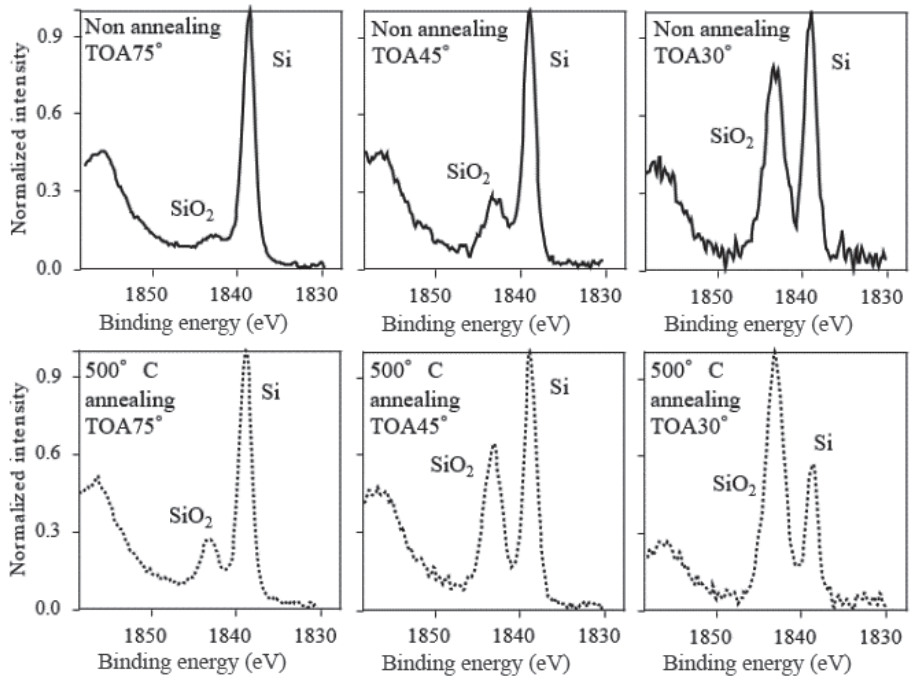

Fig. 11 Si 1s HAXPES spectra before annealing (top) and after annealing at 500 °C (bottom). From left: TOA 75°, 45°, 30°.

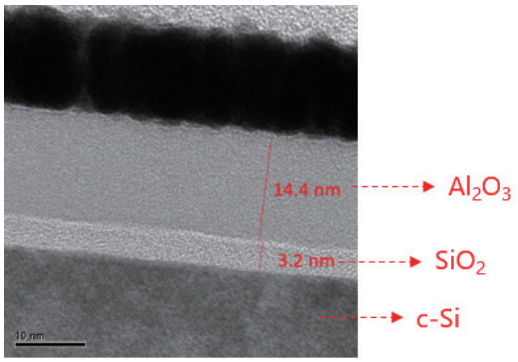

Fig. 12 TEM image of Al_2O_3-SiO_2-Si after 500 °C annealing.

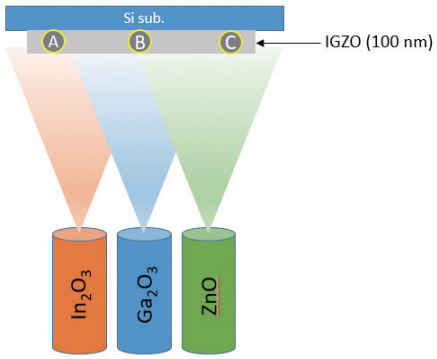

Fig. 13 Image diagram of sample preparation and measurement points.

is approximately 15 nm thick, and neither the interface nor the substrate Si can be detected using the Al Kα XPS. Furthermore, attempting sputtering can cause reduction, making chemical state analysis difficult. Therefore, the chemical state at the interface was evaluated by using Cr Kα HAXPES without sputtering.

With the Cr Kα X-ray source, it is possible to measure not only Si 2p but also Si 1s. The kinetic energy of Si 2p when measured with Al Kα radiation is approximately 1,380 eV, while that of Si 1s when measured with Cr Kα radiation is approximately 3,573 eV, meaning that the detection depth of Si 1s is greater than that of Si 2p. Therefore, using Si 1s, as in this case, makes it is possible to measure buried interfaces without the need for sputtering.

Fig. 11 shows a normalized display of the angle-resolved Si 1s spectra obtained by using the Cr Kα X-ray source for both the unannealed sample and the sample annealed at 500°C, and when measured at take-off angles of 75°, 45° and 30°. When comparing the proportions of Si and SiO_2, the proportion from the passivation layer (SiO_2) was greater at the shallow take-off angle of 30°, while the proportion from the substrate Si was greater at the larger angle of 90°. Meanwhile, comparison of the unannealed sample and the sample annealed at 500°C revealed that the amount of SiO_2 at each angle was higher after the annealing at 500°C. This indicates that annealing increases the thickness of SiO_2. Angle-resolved measurement of the sample annealed at 500°C revealed that the thicknesses of Al_2O_3 and SiO_2 were 14 nm and 3.1 nm, respectively. Fig. 12 shows a cross-sectional image of the sample obtained using a transmission electron microscope (TEM). The film thicknesses calculated from the TEM observation results were 14 nm for Al_2O_3 and 3.2 nm for SiO_2. From these results, the film thicknesses could be calculated with high accuracy using angle-resolved HAXPES measurement.

3.3 Semiconductor materials (IGZO films: indium gallium zinc oxide)

Indium (In) gallium (Ga), zinc (Zn) and oxygen (O) (IGZO) films are attracting attention as materials for next-generation thin film transistors (TFTs) due to their transparency, flexibility and high carrier mobility. However, maintaining carrier mobility and ensuring reliability are major challenges for practical application. Until now, approaches to optimizing process control have used XPS to focus on correlations between the oxygen deficit amount and carrier density. However, there have only been a few examples of the electronic structure of the material being directly evaluated. Bandgap width has a significant impact on device performance. A wide bandgap increases the dielectric breakdown voltage, reduces leakage current and reduces power consumption. Furthermore, it transmits visible light, making it suitable for displays and touch panels, while also enhancing thermal stability, enabling sharper image display and longer device lifespan. A wide bandgap also greatly enhances device performance and can be adjusted by changing the composition ratios of elements such as In, Ga and Zn. In this analysis, we present the results of using an IGZO film with a compositional gradient across the surface of a 300 mm wafer to evaluate correlations between electronic structures. A 100 nm-thick IGZO film was deposited on a 300 mm silicon substrate by using RF magnetron sputtering and In_2O_3, Ga_2O_3 and ZnO targets. This resulted in the formation of In, Ga and Zn compositional gradients (Fig. 13). Here, REELS measurement was conducted at three points (A, B and C) in the deposition plane.

3.3.1 Bandgap evaluation using REELS and ellipsometry

Fig. 14 shows the REELS spectrum of the IGZO film surface. The bandgap corresponds to the energy value at the onset of energy loss. It was observed that the bandgap decreased in the

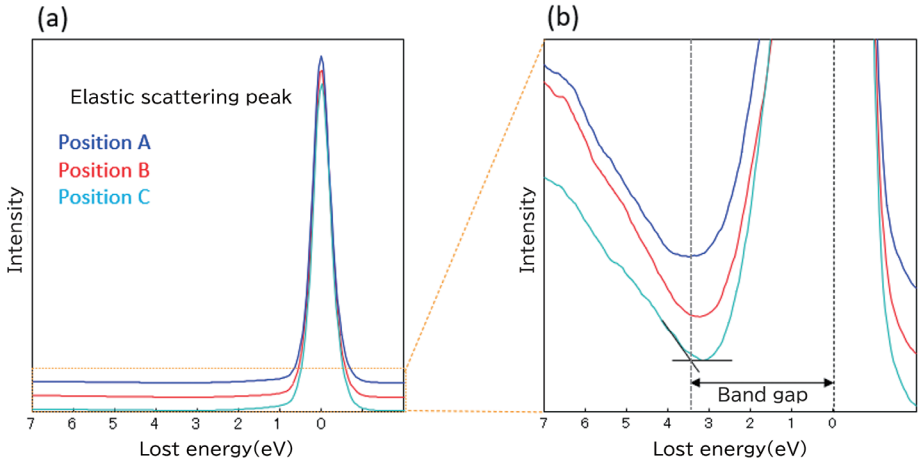

Fig. 14 REELS spectrum of the top surface. (a) Overall view (b) Enlarged view

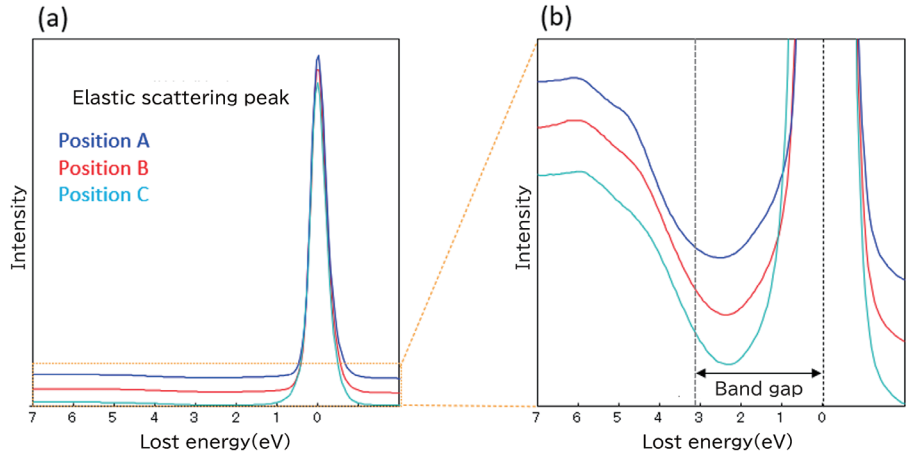

Fig. 15 REELS spectrum in the film. (a) Overall view (b) Enlarged view

Table 3 Bandgap results (eV) on the top surface and in the film. (compared with bandgap measured by ellipsometer.)

	Bandgap (eV)		
	REELS (Top surface)	REELS (in the film)	Ellipsometer (entire thin film)
Position A	3.9	3.3	3.4
Position B	3.6	3.0	3.1
Position C	3.3	2.8	2.9

order of Position A (3.9 eV), Position B (3.6 eV) and Position C (3.3 eV).

Next, Fig. 15 shows the REELS spectrum after the surface has undergone AR^+ sputtering. As shown in Table 3, the bandgap in the film decreased in the order of Position A (3.3 eV), Position B (3.0 eV) and Position C (2.8 eV). These values exhibit a very strong correlation with the bandgap values obtained using an ellipsometer, which measured the entire 100 nm thickness of the IGZO film, indicating that the measurements are highly reliable. Furthermore, the bandgap in the film was found to be smaller than that at the top surface, indicating differences in composition, chemical state, and electrical properties between the surface and inside of the film.

When developing materials, it is important to accurately understand both the surface and inside of the film. Thus, we were able to confirm that REELS enables clear identification of differences in bandgap between the top surface and inside of the film.

3.4 OLED materials

Organic electroluminescence (OLED) devices are expected to be used for video displays and low-cost displays due to their features such as luminous efficiency, flexibility, light weight and fast response. With properties such as these, their use in next-generation displays and as a lighting technology are being explored. However, practical application will require reductions in power consumption, improvements in luminous efficiency, longer device service lives, and the development of low-cost, high-yield manufacturing processes.

When designing devices, it is important to properly evaluate and optimize the electronic structure of the materials. In particular, the evaluation of the energy levels of the lowest unoccupied molecular orbitals (LUMO) and highest occupied molecular orbitals (HOMO) is useful for controlling carrier injection efficiency and recombination efficiency. This allows for the flow of electrons and holes to be optimized, enabling exciton confinement in the emission layer and improving luminous efficiency. In addition, innovative interface designs may bring about further improvements in luminous efficiency and device service life.

Carrier injection efficiency and luminescence efficiency can be improved by appropriately controlling the energy levels of LUMO and HOMO, leading to improved device performance.

During measurements, materials typically used in organic devices such as OLEDs were used as samples, as shown in Fig. 16.

① C_{60} thin film (10 nm) / Au (100 nm) / ITO (100 nm) / glass substrate

② CuPc (copper phthalocyanine) thin film (10 nm) / ITO (100 nm) / glass substrate

③ α-NPD (N,N′-bis(1-naphthyl)-N,N′-diphenyl-1,1′-biphenyl-4,4′-diamine) thin film (10 nm) / ITO (100 nm) / glass substrate

To suppress the effects of surface accumulated charging, the sample was prepared by forming a 10 nm thin film on a 100 nm ITO substrate.

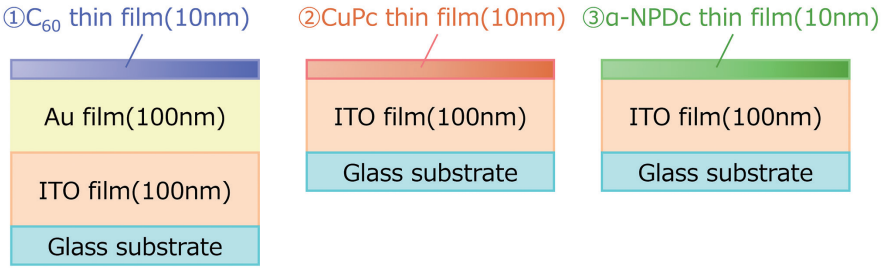

Fig. 16 Various organic EL materials.

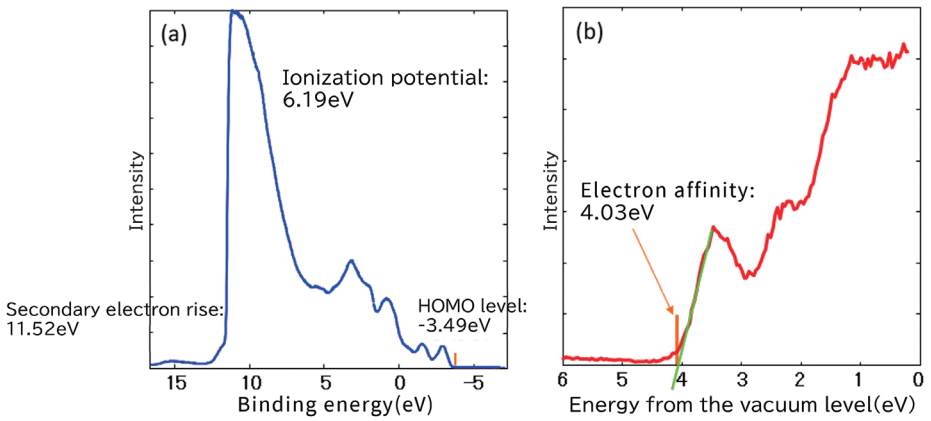

Fig. 17 Top surface spectrum of C_{60} thin film.
(a) UPS Spectrum (-5 V bias voltage applied to sample), (b) LEIPS Spectrum

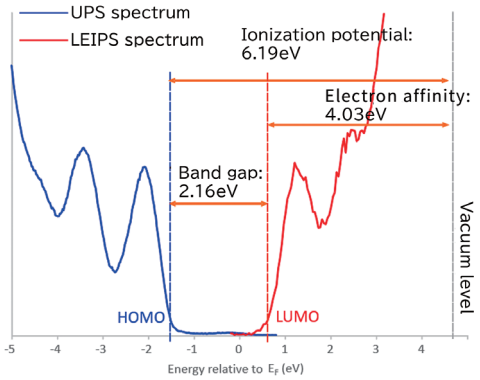

Fig. 18 UPS and LEIPS spectra of C_{60} thin film surface.

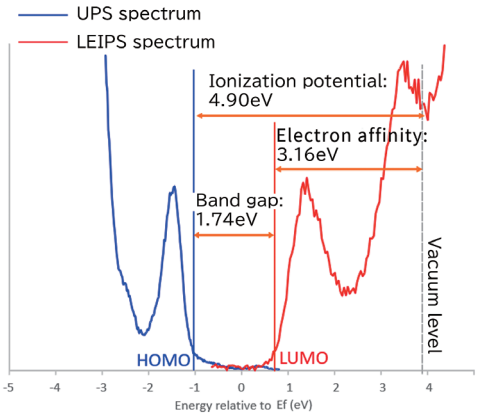

Fig. 19 UPS and LEIPS spectra of CuPc thin film surface.

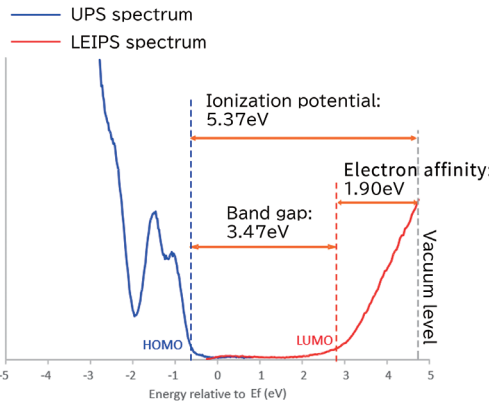

Fig. 20 UPS and LEIPS spectra of α-NPD thin film surface.

Here, we introduce a case in which the electron affinity, the top end of the valence band, and the ionization energy were calculated by using LEIPS and UPS, with the bandgap being calculated from the results of both.

3.4.1 Evaluation of OLED device band structures using UPS/LEIPS

Fig. 17 (a) shows the surface spectrum of the C_{60} thin film obtained by means of UPS. Ionization energy can be calculated from the UPS spectrum by the following equation.

Ionization energy = hν − (Eo−E_{VBM})

(hν: excitation source He I beam (21.22 eV), Eo: secondary electron onset, E_{VBM}: HOMO)

Fig. 17 (b) shows the surface spectrum of the C_{60} thin film obtained by means of LEIPS. Using the LEIPS spectrum, electron affinity can be calculated by identifying the onset position in the spectrum plotted with the horizontal axis referenced to the vacuum level.

The bandgap can be calculated by combining the UPS and LEIPS spectra, using the vacuum level as the reference (Fig. 18). Similarly, evaluation results for the CuPc thin film and the α-NPD thin film are shown in Figs. 19 and 20, respectively. LUMO levels of the thin film were determined by using the LEIPS spectrum, with the HOMO levels and Fermi levels of the thin film layer being determined by using the UPS spectrum. These results confirm that the band structure of organic/inorganic structures can be directly evaluated.

4. Summary

ULVAC-PHI PHI GENESIS is a multi-technique surface analysis platform, integrating XPS, HAXPES, AES, UPS, LEIPS, and REELS. Application examples using these techniques are presented.

References

1) Hiromichi YAMAZUI, Risayo INOUE, Noriaki SANADA and Katsumi WATANABE: JSSSJ., **37**, 150 (2016).
2) Shin-ichi IIDA, Gregory L. FISHER and Takuya MIYAYAMA: Surf. Interface Anal., **55**, 209 (2023).
3) Masahiro TERASHIMA, Kazutoshi MAMIYA and Shin-ichi IIDA: Surf. Interface Anal., **55**, 536 (2022).
4) Masahiro TERASHIMA, Kazutoshi MAMIYA, Atsuo ONO, Takahito KIMOTO, Shunsuke SASAKI and Shin-ichi IIDA: J. Vac. Soc. Jpn., **9**, 66 (2023).